Echoes in x-ray speckles track nanometer-scale plastic events in colloidal gels under shear

Michael C. Rogers, Kui Chen, Lukasz Andrzejewski, Suresh Narayanan, Subramanian Ramakrishnan, Robert L. Leheny, and James L. Harden

Phys. Rev. E **90**, 062310 — Published 22 December 2014

DOI: 10.1103/PhysRevE.90.062310

Echoes in x-ray speckles track nanometer-scale plastic events in concentrated colloidal gels under shear

Michael C. Rogers,[1,*] Kui Chen,[2] Lukasz Andrzejewski,[1] Suresh Narayanan,[3]
Subramanian Ramakrishnan,[4] Robert L. Leheny,[2,†] and James L. Harden[1,‡]

[1]*Department of Physics, University of Ottawa,*
Ottawa, Ontario, K1N 6N5, Canada
[2]*Department of Physics and Astronomy,*
Johns Hopkins University, Baltimore, Maryland 21218, USA
[3]*X-Ray Science Division, Argonne National Laboratory, Argonne, Illinois 60439, USA*
[4]*Department of Chemical and Biomedical Engineering,*
FAMU-FSU College of Engineering, Tallahassee, FL 32312, USA

(Dated: December 4, 2014)

Abstract

We report x-ray photon correlation spectroscopy experiments on a concentrated nanocolloidal gel subject to *in situ* oscillatory shear strain. The strain causes periodic echoes in the speckle pattern that lead to peaks in the intensity autocorrelation function. Above a threshold strain that is near the first yield point of the gel, the peak amplitude decays exponentially with the number of shear cycles, signaling irreversible particle rearrangements. The wave-vector dependence of the decay rate reveals a power-law distribution in the size of regions undergoing shear-induced rearrangement. The gel also displays strain softening well below the threshold, indicating a range of strains at which the rheology is nonlinear but the microscopic deformations are reversible.

PACS numbers: 83.60.La,62.20.F,83.85.Hf,82.70.Gg

*michael.rogers@uottawa.ca
†leheny@jhu.edu
‡jharden@uottawa.ca

I. INTRODUCTION

Any solid subjected to applied stress possesses an elastic limit above which it yields. Signatures of yield at the nano-to-microscale are irreversible changes to the material's structure. In amorphous solids – such as glasses, pastes, and gels – the intrinsic disorder makes identifying these microstructural changes difficult. Despite recent progress, particularly on yielding of glasses [1–4], understanding the microstructural dynamics associated with the transition from elastic response at low strain to nonlinear deformation and flow at high strain in disordered solids remains incomplete. Formulating such connections between microscopic properties and macroscopic mechanical response is a central challenge for soft-matter physics. In this paper, we present an experimental approach that exploits the capabilities of coherent x-ray scattering with *in situ* shear to reveal details about the nanometer-scale structural dynamics of soft disordered solids underlying their bulk mechanical response.

Conventional small-angle x-ray and neutron scattering under *in situ* shear has provided information about the average structural modifications of soft materials due to stress and flow [5–16]. However, a full understanding of the interdependence of microscopic properties and macroscopic rheology requires *in situ* information about the structural *dynamics* driven by stress. An ideal technique for probing such dynamics is x-ray photon correlation spectroscopy (XPCS), wherein fluctuations in coherent scattering intensity, or speckle patterns, directly monitor dynamical evolution in the microstructure. For a solid-like amorphous sample subject to an oscillatory shear strain in an XPCS measurement, the motion of constituent particles due to the strain will cause a decay in the intensity autocorrelation function $g_2(q,t)$, where q is the scattering wave vector. If the deformation is elastic and reversible, the scattering particles will return to their original position after a complete strain cycle, causing the speckle pattern to recover its original configuration. These 'echoes' in the speckle pattern will cause $g_2(q,t)$ to return to $g_2(q,0)$, and the correlation function will peak at integer multiples of the oscillation period. However, if shearing induces irreversible rearrangements so that some particles fail to return to their original positions, the echo peak will be attenuated, providing a measure of the microscopic irreversibility.

A similar approach to measure echoes with diffusing wave spectroscopy (DWS) – dynamic light scattering in the highly multiply scattering limit – has been used to investigate shear-driven structural dynamics in foams, colloidal glasses, and other soft materials [17–

22]. Recently, Laurati *et al.* reported a DWS study on concentrated colloidal gels under *in situ* oscillatory shear that showed evidence for plastic rearrangements correlated with the initial yielding of the gels [22]. Due to the multiple scattering in DWS, the technique is sensitive to motions over essentially a single length scale, which in Ref. [22] was approximately the particle radius. Here, we report XPCS experiments measuring shear echoes to track the irreversible rearrangements underlying the nonlinear rheology of a model concentrated nanocolloidal gel. Beyond providing nanometer-scale resolution of yielding behavior in the gel, the wave-vector dependence of $g_2(q,t)$ gives information about the shear-induced rearrangements over a range of length scales, thereby providing unique insight into the spatial-size distribution of the irreversible rearrangements.

II. MATERIALS ANS METHODS

A. Gel Characteristics

The gel was comprised octadecyl-grafted silica nanocolloids with radius $R \simeq 16$ nm and colloid volume fraction $\phi = 0.3$. This volume fraction places the gel in the moderately concentrated regime, above the dilute regime ($\phi \lesssim 0.1$) where gel structures have fractal character but below the crossover to the attractive glass regime, which is thought to be around $\phi \sim 0.4$ [23]. The colloids were in the solvent decalin with added polystyrene with radius of gyration $R_g \simeq 3.5$ nm and concentration $c_p/c_p^* = 0.20$, where c_p^* is the overlap concentration. The nanoparticles experience an entropic depletion attraction due to the presence of the nonabsorbing polymer that causes them to form a gel at this ϕ and c_p/c_p^*. Specifically, for these values of R_g/R and ϕ, the gel transition occurs at a polymer concentration $c_p/c_p^* \simeq 0.09$ [24], so the gel in the experiment was far from the fluid-gel boundary.

The phase behavior, structure, and bulk mechanical properties of such nanocolloidal depletion gels are well characterized [24–26]. Furthermore, these gels were employed in a previous XPCS study to track microscopic dynamics of recovery following a pre-imposed fluidizing shear [27]. The shear modulus, $G^*(\nu) = G'(\nu) + iG''(\nu)$, of the gel, shown in Fig. 1(a) as a function of strain amplitude γ at frequency $\nu = 0.318$ Hz, possesses nonlinear characteristics typical of soft disordered solids. At low γ, G' and G'' are roughly constant

with $G' >> G''$, indicating a solid-like elastic response. At larger γ, G' decreases rapidly and eventually crosses G'' indicating viscoplastic flow.

Figure 1(b) shows the strain dependence of the product $G'\gamma$, known as the elastic stress, which is a representation of the strain-dependent rheology that facilitates identification of points of yielding [28]. Above a linear regime at low strain, where the $G'\gamma$ is proportional to γ, the stress-strain relation becomes sublinear, and $G'\gamma$ reaches a local maximum near $\gamma = 5\%$. Such maxima are common in the rheology of disordered soft solids, including in depletion gels similar the one in the current study [28], and their position is often used to locate the yield point. In fact, the nonlinear rheologies of attractive colloidal glasses and concentrated colloidal gels has been shown to display two such features as a function of strain, which are identified as two separate yielding processes in these materials [28–30]. For concentrated colloidal gels like in the present study, the second yield point is seen only above $\gamma = 100\%$, and hence outside the range shown in Fig. 1 [30]. As described below, the irreversible rearrangements that affect the XPCS shear echoes become apparent at strains near the first yield point at $\gamma \approx 5\%$, which is associated with initial bond-breaking events [28, 29]. Hence, we focus on the behavior at these smaller strains. Presumably, a second yielding process like that seen previously, which has been associated with cage breakup in the case of denser colloidal systems and cluster breakup in less dense systems [28, 29], would be apparent in measurements on the gel that extended to $\gamma > 100\%$

B. XPCS with *in situ* Shear

To investigate the nanoscale structural rearrangements corresponding to the nonlinear rheology, we conducted small-angle XPCS experiments under *in situ* shear. Measurements were performed with a custom shear cell at beamline 8-ID-I of the Advanced Photon Source using 7.34 keV x-rays. The gel was contained between parallel diamond windows with 500 μm spacing. A thin sheet of polyamide was attached to each window and was roughened to prevent wall slip. One window was held static, and the other was attached to a stage that was translated by a voice-coil linear actuator. An optical encoder with 50-nm precision, zero reference, and 32 kHz refresh rate was attached to the translating stage to enable precise application of arbitrary, time-dependent shear strains through computer control of the actuator. A 20×20 μm^2 partially coherent beam was incident on the sample normal to

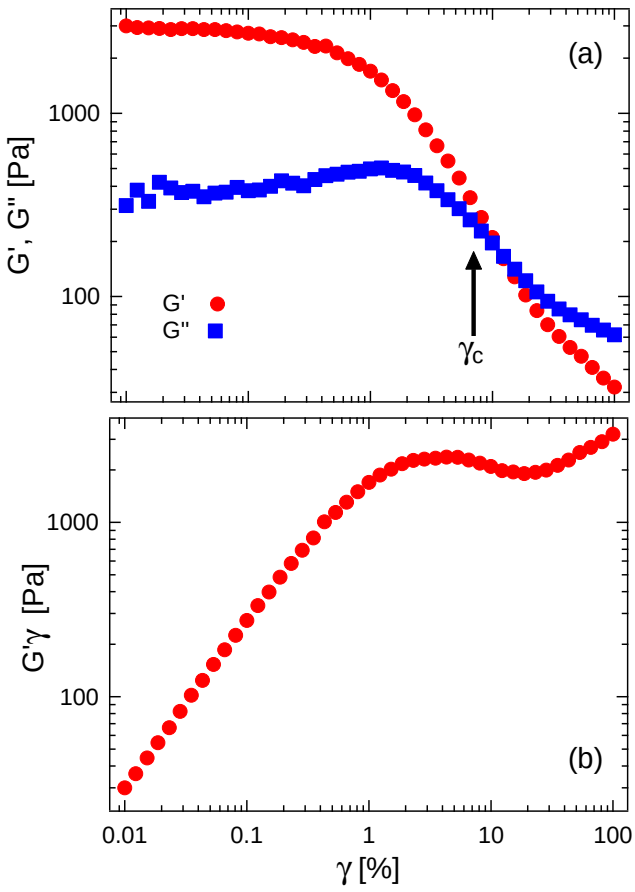

FIG. 1: (color online) (a) Storage (red circles) and loss (blue squares) modulus and (b) the elastic stress at $\nu = 0.318$ Hz as a function of strain amplitude. The arrow in (a) indicates the threshold strain above which the XPCS shear echo amplitude displays pronounced attenuation.

the windows, and measurements of the coherent scattering were made in transmission. This configuration made the incident beam parallel to the shear-gradient direction, so that in the small-angle-scattering limit of the measurements the scattering wave vectors lay in the flow-vorticity plane. A direct-illuminated CCD area detector (Princeton Instruments, 1300×1340 pixels) located 4.07 m after the sample measured the scattering intensity over wave-vector magnitudes $0.03\ \mathrm{nm}^{-1} < q < 0.22\ \mathrm{nm}^{-1}$ and wave-vector directions that spanned the flow and vorticity directions. For analysis, the detector pixels were partitioned according to q magnitude and direction with $\sim 10^3$-10^4 pixels (where speckle size ≈ 1 pixel) in each partition to assure proper ensemble averaging. Figure 2 shows an example of a CCD image of the scattering intensity from the gel with two such partitions highlighted.

A schematic representation of the oscillatory strain profile applied during the measurements is shown in Fig. 3. The strain followed a sinusoidal time dependence between extrema in its value. At each extremum the strain was held constant for a short period during which a scattering image was obtained. Periodically holding the strain fixed in this way eliminated "smearing" of the speckle pattern due to shearing during the x-ray exposures. In most cases, a measurement at a given strain amplitude and oscillation frequency included 256 images (128 oscillation periods) from which $g_2(q,t)$ was determined. Prior to each measurement, several periods of oscillation were applied to avoid any transient effects. By analyzing the first half of the images and the second half separately (*i.e.*, by calculating $g_2(q,t)$ from the first 128 frames and from the second 128 frames separately), we confirmed that no systematic changes in the correlation function occurred during the measurement, indicating that the measurements probed the steady-state behavior under oscillatory shear. In addition, measurements of $g_2(q,t)$ under quiescent conditions were performed before and after the measurements under shear, and no systematic effects from intervening shearing, such as shear-induced rejuvenation, were observed for any of the shear profiles applied in the experiment (strain amplitudes $\gamma \leq 30\%$). This robustness is consistent with previous studies of these depletion gels that showed the rheology and microstructure recovered essentially immediately after cessation of applied shear [31]. We also repeated several measurements during the course of the experiment. The repeated measurements showed good agreement, indicating that no shear-driven sample evolution.

We note that the brief interruptions at the strain extrema for obtaining the x-ray images potentially complicate comparisons of the echo results with rheology and (incoherent) scattering studies that employ large amplitude oscillatory shear (LAOS) to investigate the nonlinear response of colloidal gels [12–14, 22, 28]. However, we believe these complications are minor and valid comparisons can be made. Studies have shown that concentrated gels formed from colloids with short-range attraction obey the "Delaware-Rutgers" rule [13], which states that for yielding concentrated suspensions with a large structural relaxation times, the response during oscillatory deformation is dictated by the maximum shear rate (frequency times strain amplitude) rather than the frequency of deformation [32]. Hence, for comparisons with LAOS measurements, one should consider the magnitude and the period of the sinusoidal part of the strain (neglecting the interruption) in the XPCS measurements.

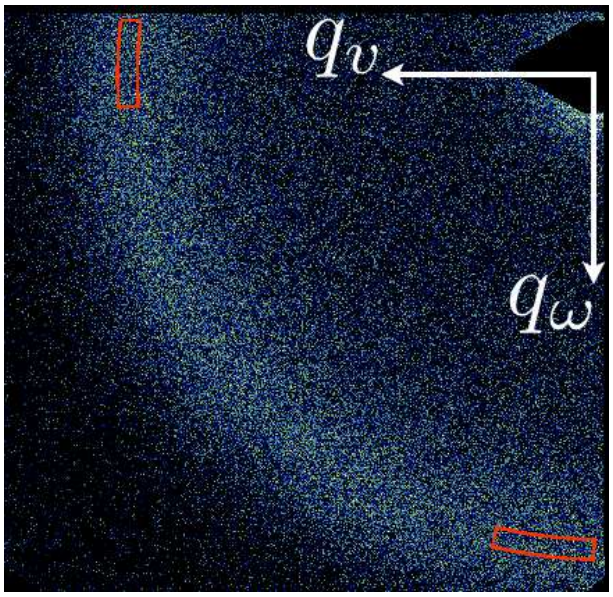

FIG. 2: (color online) CCD image of the x-ray scattering intensity. The incident beam position, corresponding to $q = 0$, is obscured by the shadow of the beamstop in the upper right. The wave vector directions parallel to the flow direction q_v and parallel to the vorticity direction q_ω are indicated by arrows. Two examples of partitions delineating the pixels included analysis of $g_2(q,t)$ at fixed wave-vector magnitude and direction are shown by the red boxes. These two partitions are located at $q = 0.19$ nm^{-1}.

III. RESULTS

Figure 4 displays examples of the intermediate scattering function $g_2(q,t)$ during application of strain profiles with amplitudes $\gamma = 4\%$ and 12% at $q = 0.18$ nm^{-1}, a wave vector near the interparticle structure factor peak in the scattering intensity, in a direction parallel to the vorticity direction. The strain rate between extrema corresponded to a sine wave with frequency 0.318 Hz, and the hold time at each extremum was 0.5 s, during which a 0.25 s x-ray exposure was obtained, leading to a repeat time for the strain of $T = 4.14$ s. For comparison, $g_2(q,t)$ measured in the absence of shear is also shown. In this quiescent state, $g_2(q,t)$ has a shape common to many disordered soft solids in which it maintains a large value at short delay times t, indicating a nominally static configuration, but decays at long delay times ($t \gtrsim 100$ s) with a compressed-exponential form that can be associated with slow relaxation of heterogeneous residual stress [33–37]. For the measurements under

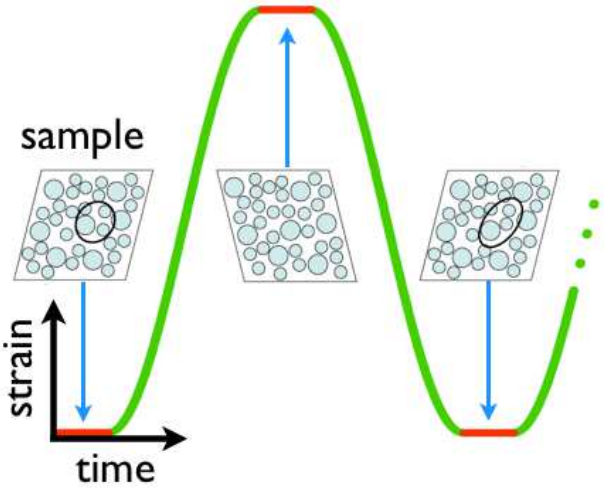

FIG. 3: (color online) Schematic of the oscillatory strain profile and microstructural response. The strain followed a sinusoidal form (green) between extrema. At each extremum the strain was held constant for a short time (red) during which a coherent x-ray exposure was obtained. The cartoons of the amorphous solid illustrate the change in strain each half-period and the recovery of the microstructure each full period. The circled particles highlight a region that undergoes irreversible rearrangement during the cycle.

in situ shear, $g_2(q,t)$ displays periodic peaks corresponding to echoes in the speckle pattern. As illustrated schematically in Fig. 3, the change in strain between extrema leads to gradients in the particle displacements that alter the speckle pattern completely [38, 39] even for modest values of strain. Thus, $g_2(q,t) \approx 1$ at $t = (n + 1/2)T$, where n is an integer. However, at delay times separated by an integer number of repeat times, $t = nT$, the strain returns and the speckle pattern is recovered, causing $g_2(q,t)$ to increase above one. At $\gamma = 4\%$, $g_2(q, t = nT)$ traces $g_2(q,t)$ measured under quiescent conditions, indicating that the particles undergo no shear-induced irreversible rearrangements. At $\gamma = 12\%$, $g_2(q, t = nT)$ decays rapidly, revealing significant irreversible rearrangement in the gel.

Figure 5 displays $g_2(q, t = nT)$ at $q = 0.18$ nm^{-1} along the vorticity direction at several γ as a function of the number of "delay cycles" n. (We emphasize that $g_2(q,n)$ is a measure of the speckle correlations in images separated by n periods of oscillation in steady state.) The attenuation of the echo peaks increases sharply between $\gamma = 6\%$ and 8%, indicating a transition to irreversible, nanoplastic deformation above a threshold strain, $\gamma_c \approx 7\%$.

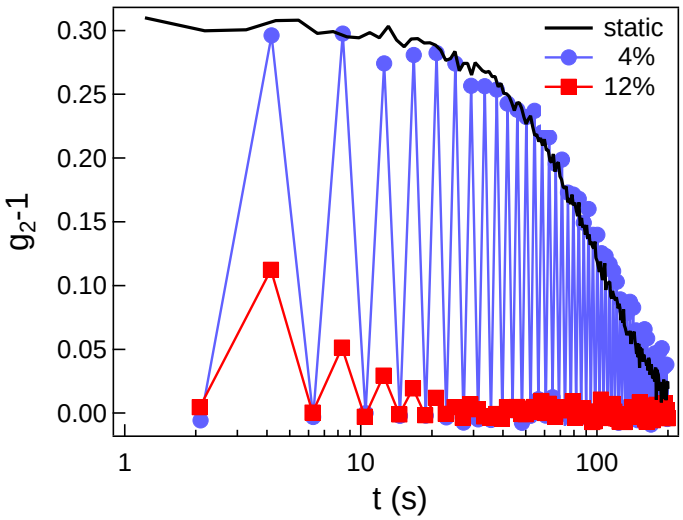

FIG. 4: (color online) Echoes in the intensity autocorrelation function during application of oscillatory strain with amplitudes $\gamma = 4\%$ (blue circles) and 12% (red squares) measured in the vorticity direction at $q = 0.18$ nm^{-1}. The applied strain between extrema followed to a sine wave with frequency 0.318 Hz and the hold time at each extremum was 0.5 s, leading to repeat time of 4.14 s. The blue and red lines are guides to the eye. The echoes at $\gamma = 4\%$ track the intensity autocorrelation of the quiescent gel (black line), indicating that shear plays no role in decorrelation at this strain amplitude.

The arrow in Fig. 1 indicates the approximate value of γ_c. $G'(\nu)$ displays significant strain softening at considerably lower γ, revealing a range of strains that cause nonlinear but fully reversible deformations. Studies of glasses and granular materials have observed that reversible plastic events are prevalent at strains below those causing irreversible events, and in some cases these events can be linked to the onset of nonlinear stress response [2, 4, 40, 41]. Our results on the nanocolloidal gel – an attractive system – indicate that this behavior is general to both repulsive and attractive systems. Also shown in Fig. 5 are the echo peak amplitudes at one strain above the threshold ($\gamma = 12\%$) for q parallel to the flow direction. Surprisingly, the attenuation is anisotropic, with the echoes decaying more rapidly as a function of n for q along the vorticity direction than along the flow direction; however, the results along both directions indicate $\gamma_c \approx 7\%$ for the onset of irreversibility.

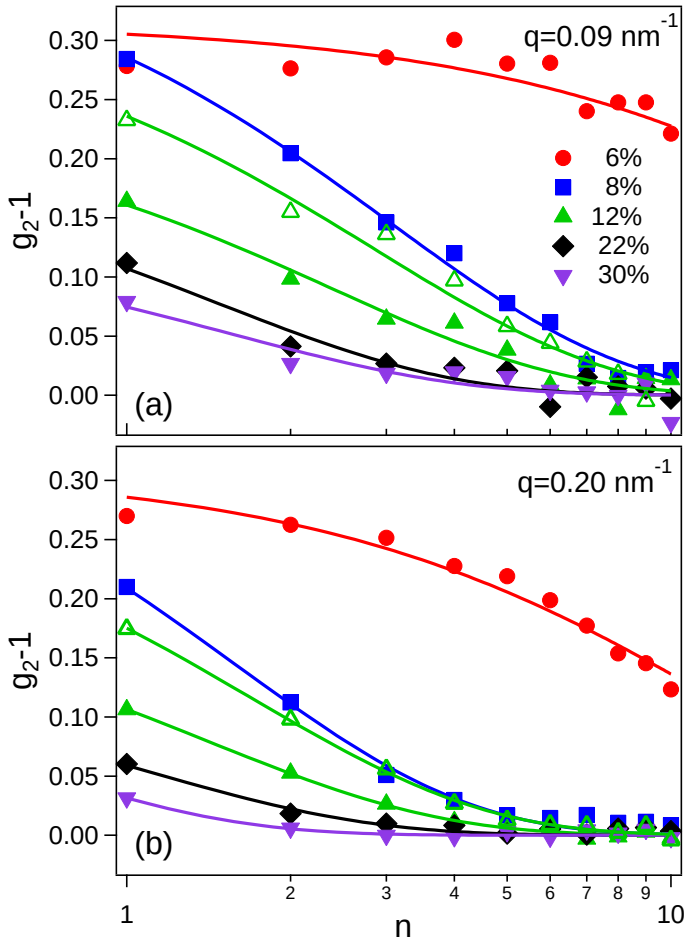

FIG. 5: (color online) Echo peak amplitudes at wave vectors along the vorticity direction at (a) $q = 0.09$ nm^{-1} and (b) $q = 0.20$ nm^{-1} as a function of delay cycle for strains γ=6% (red circles), 8% (blue squares), 12% (green triangles), 22% (black diamonds), and 30% (purple inverted triangles). Also shown are the amplitudes at γ=12% along the flow direction (open green triangles). Solid lines are the results from fitting an exponential decay to the echo-peak amplitude.

The solid lines in Fig. 5 are results from fitting exponential decays to the peak amplitudes,

$$g_2(q, n) = 1 + \beta \exp(-\Gamma \cdot n). \tag{1}$$

where $\beta \simeq 0.30$ is the Siegert factor determined from a separate measurements on a static sample (aerogel). We find an exponential decay accurately describes the peak amplitudes at all γ and q, both in the flow and vorticity directions, for which the decay is sufficiently rapid to dominate the intrinsic, quiescent decay in $g_2(q, t)$. Figure 6 shows the decay rate

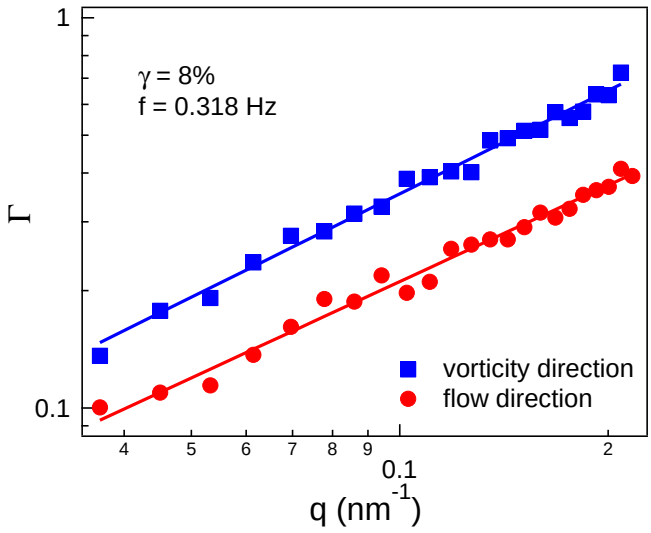

FIG. 6: (color online). Echo decay rate Γ (in 1/cycles) at $\gamma = 8\%$ as a function of wave-vector amplitude for wave vectors in the flow direction (red circles) and the vorticity direction (blue squares). Solid lines indicate the result of power-law fits, which give exponents $\alpha = 0.82 \pm 0.03$ (red) and $\alpha = 0.88 \pm 0.03$ (blue).

Γ as a function of wave vector amplitude at $\gamma = 8\%$ for q parallel to the flow and vorticity directions. Consistent with the results in Fig. 5, the rate is larger along the vorticity direction than along the flow direction, perhaps due to subtle effects of gravity along the vorticity direction. However, the static scattering intensity $I(q)$, shown in Fig. 7 for q along the two directions, is fully isotropic, indicating no corresponding signatures of shear-induced anisotropy in the structure. In both q directions, the decay rate scales as a weak power law with wave vector, $\Gamma(q) \sim q^{\alpha}$ with $\alpha = 0.82 \pm 0.03$ in the flow direction and $\alpha = 0.88 \pm 0.03$ in the vorticity direction, as shown by the power-law fits in Fig. 6. Such power-law behavior is seen at all γ for which Γ could be accurately determined. Although the value of α varied somewhat between measurements, perhaps due to sample heterogeneity, it showed no clear systematic dependence on strain profile. The average value was $\alpha = 0.7 \pm 0.2$

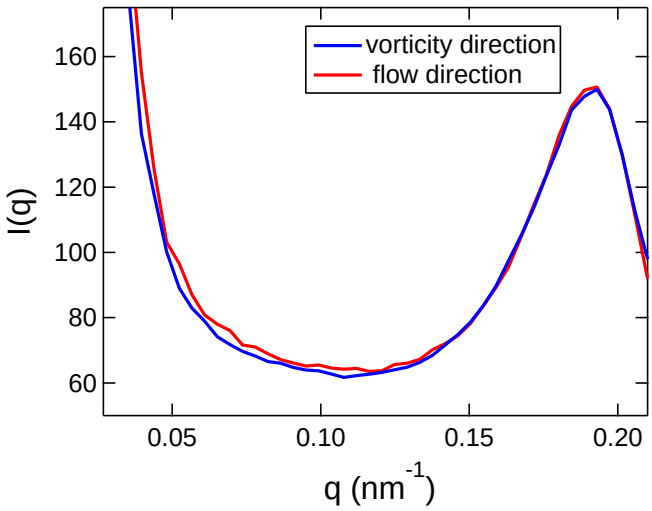

FIG. 7: (color online). Static x-ray scattering intensity as a function of q along the flow (red) and vorticity (blue) directions at $\gamma = 8\%$.

IV. DISCUSSION

A. Length scale of structural response to shear

As Fig. 7 demonstrates, the imposed oscillatory shear creates no noticeable anisotropy in the gel structure over the range of wave vectors probed with small angle x-ray scattering. A prominent structural signature seen in dilute gels in the fractal regime ($\phi < 0.1$) is the formation of large-scale shear-induced anisotropies that manifest distinct scattering profiles known as "butterfly" patterns at lower q in static light scattering [15, 16]. (These patterns can also be observed for gels with larger concentration in the higher-q range of small angle x-ray and neutron scattering but only at considerably larger strain amplitudes than those probed here [13].) While we cannot completely rule out such large-length scale structural response in the concentrated gel under study, we believe it is unlikely. As Vermant and coworkers have shown in a study on yielding in two-dimensional gels [42], the characteristic scale of structural deformations becomes increasingly localized as gel concentration increases, and the typical spatial scale is only a few particle diameters in the concentrated regime. Further, effective theories based on mode coupling ideas have successfully predicted many features of yielding in concentrated colloidal gels [43, 44]. These theories consider only

local structural properties, specifically those contained in the static structure factor $S(q)$, and issues such as large-scale heterogeneity, the connectivity of the gel structure, and bond percolation are not taken into account. Hence their success suggests that these nonlocal properties ultimately have only weak effect on the structural dynamics associated with yielding in concentrated gels. Finally, the motion associated with the rigid rotation of large scale clusters like that pictured to create the anisotropic low-q scattering profiles at lower concentration would cause immediate complete decorrelation of $g_2(q, n)$ in the range of q accessed with XPCS, in stark contrast to what we observe. Thus, from the structural and dynamical information provided in this XPCS study, we can infer that the shear-induced structural response of the concentrated gels near the first yield point involves primarily small-scale structural rearrangements.

B. Model for the shear-induced structural dynamics

The observed exponential decay in $g_2(q, n)$ provides insight into the nature of the irreversible rearrangements underlying the nonlinear mechanical behavior of the gel. In particular, the fact that $g_2(q, n)$ decays fully to one with no sign of persistent correlations implies that essentially the entire sample within the scattering volume eventually undergoes irreversible rearrangement as a consequence of the shear. That is, when viewed over multiple shear cycles, the irreversible rearrangements are not isolated to a portion of the sample as one might expect, for example, with shear banding.

One possible interpretation for such non-localized dynamics would invoke a stress-induced, effective diffusivity for the colloidal particles [45, 46]. While such motion would lead to an exponential decay in $g_2(q, n)$, the decay rate would vary with wave vector as $\Gamma \sim q^2$, perhaps modulated by the structure factor $S(q)$ in analogy with de Gennes narrowing. In contrast, the much weaker power-law dependence of Γ on q in Fig. 6, with no influence of features in $S(q)$ like the large interparticle structure-factor peak near $q = 0.19$ nm^{-1}, is incompatible with a picture of effective diffusion.

Instead, we can understand the exponential decay in $g_2(q, n)$ through a model of heterogeneous dynamics in which regions of the sample comprising a volume fraction f undergo irreversible rearrangements during a shear cycle. The coherent scattering from these regions becomes randomized, while that from the remainder of the sample remains unchanged. In

this case, the intermediate scattering function $g_1(q,t)$ – which is related to $g_2(q,t)$ though the Siegert relation, $g_2(q,t) = 1 + \beta g_1^2(q,t)$ – is a mixture of contributions from scattering from these dynamic and static components much like in a heterodyne measurement [47]. Following such a heterodyne analysis, the dynamics during a cycle leads g_1 to a decrease such that $g_1(q, n = 1) = (1 - f)g_1(q, 0)$ [47]. Further, if the regions that rearrange in a given cycle are located randomly in the sample, independent of the locations of previous events, then the fraction of sample that remains unaltered over n cycles is $(1 - f)^n$. Thus, for such rearrangements with no history, $g_1(q, n) = (1 - f)^n g_1(q, 0)$. Or, since $g_1(q, 0) = 1$,

$$g_1(q, n) = (1 - f)^n, \tag{2}$$

which leads directly to an exponential form for $g_2(q, n)$ like in Eq. (1) with $\Gamma = 2f$.

Thus, within this model the q dependence of Γ is that of $2f$. To interpret this dependence, we note any irreversible event that decorrelates g_2 at a wave vector q must cause the particles to rearrange their positions on a length scale $\ell \gtrsim q^{-1}$. Hence, if an event contributes to annenuating g_2 at some q, it does so for all larger q as well. Therefore, since $f \sim \Gamma \sim q^\alpha$, the fraction of the sample each cycle involved in events that rearrange the positions of particles over a length scale ℓ greater than some given length ℓ_0 varies as $f(\ell > \ell_0) \sim \ell_0^{-\alpha}$. Or, the fraction in which the scatterers are rearranged on a length scale ℓ scales as

$$f(\ell) \sim \ell^{-(\alpha+1)}. \tag{3}$$

This model leads to an interpretation of the anisotropy in Γ in Fig. 6: The different decay rates imply the motion within rearranging regions is on average anisotropic (larger along the vorticity direction than the flow direction), but this anisotropy is self-similar and the power-law size distributions in the two directions differ by only a scale factor.

Further, assuming the linear size of a region L undergoing rearrangement scales with ℓ, then the fraction of the sample involved in events of size L similarly varies as $f(L) \sim L^{-(\alpha+1)}$. Since each event of linear size L occupies a volume V that scales as L^3, the number of events hence scales with their linear size as $N(L) \sim L^{-(\alpha+4)}$. Thus, the number of events varies with their volume as

$$N(V) \sim V^{-(\alpha+4)/3}, \tag{4}$$

or taking $\alpha = 0.7 \pm 0.2$, $N(V) \sim V^{-\xi}$ with $\xi = 1.56 \pm 0.06$. Such a power-law distribution of event sizes indicates a nonequilibrium critical transition in the gel at yielding. Many

physical phenomena involving disorder – from earthquakes to Barkhausen noise to fluid-interface depinning – exhibit power-law statistics in their response to a driving force, and ideas of nonequilibrium critical phenomena provide a unifying perspective for this behavior. Indeed, power-law distributions have been observed in the nonlinear mechanical response in numerical simulations of glasses [48, 49] and in experiments on disordered crystals [50–52] and metallic glasses [53, 54], where the measured quantities were fluctuations in energy or stress σ that scaled as $N(\sigma) \sim \sigma^{-\tau}$ with τ in the range 1.5-1.6. The remarkably similar values of τ and the exponent ξ we obtain suggests the spatial size of plastic events scales with the energy dissipated by them, $\xi = \tau$.

V. CONCLUSION

In conclusion, measurements of the XPCS echo peaks on a concentrated colloidal gel under oscillatory shear reveal a threshold strain for irreversible particle rearrangements that is near a (first) local maximum in the elastic stress, a signature of a yield point in gel rheology. The gel also displays strain softening well below this threshold, indicating a range of strains at which the rheology is nonlinear but the microscopic deformations are reversible. This behavior has been noted previously in repulsive systems, and now this result generalizes it to systems with attractive particle interactions. Further, the wave-vector dependence of the XPCS echoes not only demonstrates that nanocolloidal gels undergo a nonequilibrium critical transition at yielding, but it also uniquely provides direct characterization of the spatial-size distribution of the critical events on a nanometer scale. An interesting future experiment would obtain both exponents ξ and τ on the same system to test the scaling between the energy and spatial-size of plastic events. More generally, the wealth of nanostructured soft solids with pronounced nonlinear rheology that are amenable to interrogation via XPCS with *in situ* shear should make further application of x-ray speckle echo an important tool for this field. Indeed, beyond accessing structural dynamics at nanometer scales, other demonstrated advantages of XPCS, such as the abilities to measure opaque samples and to interrogate heterogeneous dynamics with micrometer-sized beams, should have particular value in probing nonlinear structural response of soft materials under shear.

Acknowledgements: We thank W. Burghardt, A. Sandy, and M. Sutton for helpful dis-

cussions. This research was supported by NSF CBET-1336166, NSF HRD-1238524, and the NSERC Discovery and RTI programs. Use of the APS was supported by DOE BES under Contract No. DE-AC02-06CH11357.

---

[1] M. L. Falk and J. Langer, Annu. Rev. Condens. Matter Phys. **2**, 353 (2011).

[2] N. C. Keim and P. E. Arratia, Phys. Rev. Lett. **112**, 028302 (2014).

[3] N. V. Priezjev, Phys. Rev. E **87**, 052302 (2013).

[4] D. Fiocco, G. Foffi, and S. Sastry, Phys. Rev. E **88**, 020301 (2013).

[5] R. G. Egres, F. Nettesheim, and N. J. Wagner, J. Rheol. **50**, 685 (2006).

[6] I. Bihannic, C. Baravian, J. F. L. Duval, E. Paineau, F. Meneau, P. Levitz, J. P. de Silva, P. Davidson, and L. J. Michot, J. Phys. Chem. B **114**, 16347 (2010).

[7] M. P. Lettinga, P. Holmqvist, P. Ballesta, S. Rogers, D. Kleshchanok, and B. Struth, Phys. Rev. Lett. **109**, 246001 (2012).

[8] C. R. López-Barrón, L. Porcar, A. P. R. Eberle, and N. J. Wagner, Phys. Rev. Lett. **108**, 258301 (2012).

[9] A. M. Philippe, C. Baravian, M. Jenny, F. Meneau, and L. J. Michot, Phys. Rev. Lett. **108**, 254501 (2012).

[10] F. E. Caputo, W. R. Burghardt, K. Krishnan, F. S. Bates, and T. P. Lodge, Phys. Rev. E **66**, 041401 (2002).

[11] L. M. C. Dykes, J. M. Torkelson, and W. R. Burghardt, Macromolecules **45**, 1622 (2012).

[12] A. P. R. Eberle, N. Martys, L. Porcar, S. R. Kline, W. L. George, J. M. Kim, P. D. Butler, and N. J. Wagner, Phys. Rev. E **89**, 050302 (2014).

[13] J. Min Kim, A. P. R. Eberle, A. Kate Gurnon, L. Porcar, and N. J. Wagner, J. Rheol. **58**, 1301 (2014).

[14] J. Kim, D. Merger, M. Wilhelm, and M. E. Helgeson, J. Rheol. **58**, 1359 (2014).

[15] P. Varadan and M. J. Solomon, Langmuir **17**, 2918 (2001).

[16] H. Hoekstra, J. Mewis, T. Narayanan, and J. Vermant, Langmuir **21**, 11017 (2005).

[17] P. Hébraud, F. Lequeux, J. P. Munch, and D. J. Pine, Phys. Rev. Lett. **78**, 4657 (1997).

[18] R. Höhler, S. Cohen-Addad, and H. Hoballah, Phys. Rev. Lett. **79**, 1154 (1997).

[19] G. Petekidis, A. Moussaïd, and P. N. Pusey, Phys. Rev. E **66**, 051402 (2002).

[20] V. Viasnoff and F. Lequeux, arXiv:cond-mat/0305389.

[21] P. A. Smith, G. Petekidis, S. U. Egelhaaf, and W. C. K. Poon, Phys. Rev. E **76**, 041402 (2007).

[22] M. Laurati, S. U. Egelhaaf, and G. Petekidis, J. Rheol. **58**, 1395 (2014).

[23] A. P. R. Eberle, R. Castaeda-Priego, J. M. Kim, and N. J. Wagner, Langmuir **28**, 1866 (2012).

[24] S. A. Shah, Y.-L. Chen, K. S. Schweizer, and C. F. Zukoski, J. Chem. Phys. **119**, 8747 (2003).

[25] S. A. Shah, Y.-L. Chen, S. Ramakrishnan, K. S. Schweizer, and C. F. Zukoski, J. Phys.: Condens. Matter **15**, 4751 (2003).

[26] S. Ramakrishnan, Y.-L. Chen, K. S. Schweizer, and C. F. Zukoski, Phys. Rev. E **70**, 040401 (2004).

[27] B. Chung, S. Ramakrishnan, R. Bandyopadhyay, D. Liang, C. F. Zukoski, J. L. Harden, and R. L. Leheny, Phys. Rev. Lett. **96**, 228301 (2006).

[28] M. Laurati, S. U. Egelhaaf, and G. Petekidis, J. Rheol. **55**, 673 (2011).

[29] K. N. Pham, G. Petekidis, D. Vlassopoulos, S. U. Egelhaaf, W. C. K. Poon, and P. N. Pusey, J. Rheol. **52**, 649 (2008).

[30] N. Koumakis and G. Petekidis, Soft Matter **7**, 2456 (2011).

[31] S. Ramakrishnan, V. Gopalakrishnan, and C. F. Zukoski, Langmuir **21**, 9917 (2005).

[32] D. Doraiswamy, A. N. Mujumdar, I. Tsao, A. N. Beris, S. C. Danforth, and A. B. Metzner, J. Rheol. **35**, 647 (1991).

[33] J.-P. Bouchaud and E. Pitard, Eur. Phys. J. E **6**, 231 (2001).

[34] L. Cipelletti, L. Ramos, S. Manley, E. Pitard, D. A. Weitz, E. E. Pashkovski, and M. Johansson, Faraday Discuss. **123**, 237 (2003).

[35] A. Madsen, R. L. Leheny, H. Guo, M. Sprung, and O. Czakkel, New J. Phys. **12**, 055001 (2010).

[36] R. L. Leheny, Curr. Opin. Colloid Interface Sci. **17**, 3 (2012).

[37] L. Mohan, R. T. Bonnecaze, and M. Cloitre, Phys. Rev. Lett. **111**, 268301 (2013).

[38] A. Fluerasu, P. Kwasniewski, C. Caronna, F. Destremaut, J.-B. Salmon, and A. Madsen, New J. Phys. **12**, 035023 (2010).

[39] W. R. Burghardt, M. Sikorski, A. R. Sandy, and S. Narayanan, Phys. Rev. E **85**, 021402 (2012).

[40] S. Slotterback, M. Mailman, K. Ronaszegi, M. van Hecke, M. Girvan, and W. Losert, Phys.

Rev. E **85**, 021309 (2012).

[41] I. Regev, T. Lookman, and C. Reichhardt, Phys. Rev. E **88**, 062401 (2013).

[42] K. Masschaele, J. Fransaer, and J. Vermant, J. Rheol. **53**, 1437 (2009).

[43] V. Kobelev and K. S. Schweizer, J. Chem. Phys. **123**, 164902 (2005).

[44] V. Gopalakrishnan and C. F. Zukoski, Langmuir **23**, 8187 (2007).

[45] K. Miyazaki, D. R. Reichman, and R. Yamamoto, Phys. Rev. E **70**, 011501 (2004).

[46] R. Besseling, E. R. Weeks, A. B. Schofield, and W. C. K. Poon, Phys. Rev. Lett. **99**, 028301 (2007).

[47] F. Livet, F. Bley, F. Ehrburger-Dolle, I. Morfin, E. Geissler, and M. Sutton, J. Synchrotron Rad. **13**, 453 (2006).

[48] N. P. Bailey, J. Schiøtz, A. Lemaître, and K. W. Jacobsen, Phys. Rev. Lett. **98**, 095501 (2007).

[49] K. M. Salerno, C. E. Maloney, and M. O. Robbins, Phys. Rev. Lett. **109**, 105703 (2012).

[50] M.-C. Miguel, A. Vespignani, S. Zapperi, J. Weiss, and J.-R. Grasso, Nature **410**, 667 (2001).

[51] D. M. Dimiduk, C. Woodward, R. LeSar, and M. D. Uchic, Science **312**, 1188 (2006).

[52] M. Zaiser, Adv. Phys. **55**, 185 (2006).

[53] G. Wang, K. Chan, L. Xia, P. Yu, J. Shen, and W. Wang, Acta Mater. **57**, 6146 (2009), ISSN 1359-6454.

[54] B. A. Sun, H. B. Yu, W. Jiao, H. Y. Bai, D. Q. Zhao, and W. H. Wang, Phys. Rev. Lett. **105**, 035501 (2010).